



Article

Performance Enhancement of Vehicle Mechatronic Inertial Suspension, Employing a Bridge Electrical Network

Tianyi Zhang ¹, Xiaofeng Yang ^{1,*} , Yujie Shen ², Xiaofu Liu ³ and Tao He ¹

¹ School of Automotive and Traffic Engineering, Jiangsu University, Zhenjiang 212013, China

² Automotive Engineering Research Institute, Jiangsu University, Zhenjiang 212013, China

³ College of Engineering, China Agricultural University, Beijing 100083, China

* Correspondence: yangxf18@ujs.edu.cn; Tel.: +86-139-5285-3832

Abstract: Inerters, a new type of mass element, have been successfully applied in various fields, such as in automotive and civil engineering. The development of a new element, named a mechatronic inerter, which consists of a ball-screw inerter and permanent magnet electric machinery, proves the feasibility of adopting electrical element impedances to simulate corresponding mechanical elements. In this paper, the structures of the bridge electrical network and series-parallel electrical network and their impedance characteristics are first introduced. Then, a seven-degree-of-freedom vehicle model is established. In addition, by comparison with passive suspension, a bridge network and a series-parallel network with various basic topologies are used to improve the vibration isolation performance of mechatronic inertial suspension, and the advantages of the bridge network (a) are demonstrated. Finally, a bridge electrical network (a) was designed and a real vehicle test was carried out. The test results showed that the mechatronic inertial suspension based on the bridge network (a) was superior to the passive suspension; the RMS (root-mean-square) values of the suspension working space and dynamic tire load of the left rear wheel suspension were reduced by 21.1% and 6.3%, respectively; and the RMS value of the centroid acceleration was improved by 1.8%.

Keywords: suspension; mechatronic inerter; bridge network; high-order impedance; real vehicle test



Citation: Zhang, T.; Yang, X.; Shen, Y.; Liu, X.; He, T. Performance Enhancement of Vehicle Mechatronic Inertial Suspension, Employing a Bridge Electrical Network. *World Electr. Veh. J.* **2022**, *13*, 229. <https://doi.org/10.3390/wevj13120229>

Academic Editors: Yong Li, Xing Xu, Lin Zhang, Yechen Qin and Yang Lu

Received: 29 October 2022

Accepted: 23 November 2022

Published: 1 December 2022

Publisher's Note: MDPI stays neutral with regard to jurisdictional claims in published maps and institutional affiliations.



Copyright: © 2022 by the authors. Licensee MDPI, Basel, Switzerland. This article is an open access article distributed under the terms and conditions of the Creative Commons Attribution (CC BY) license (<https://creativecommons.org/licenses/by/4.0/>).

1. Introduction

Vehicle suspension has gradually developed from passive suspension with fixed parameters, to semi-active suspension with variable parameters [1], and active suspension with active control [2]. However, the suspension structure still utilizes a “spring–damper” system, which are connected in parallel, and the improvement of suspension performance has encountered a bottleneck. Since Smith proposed the inerter in 2002 [3], the inerter-based vibration suppression system has been a popular direction in mechanical fields and has successfully made up for a lack of inertial element and promoted the structural development of vehicle suspension. This article refers to suspension with an inerter as inertial suspension. With the rapid development of inertial suspension systems, the inerter has developed various implementation forms. Papageorgiou et al. introduced a rack-and-pinion inerter in 2009 [4], Faraj proposed a ball-screw inerter in 2019 [5], and Liu designed a hydraulic inerter in 2018 [6]. Other inerters have been proposed by scholars, such as a fluid inerter [7,8] and hydraulic electric inerter [9]. Inertial suspension performs better than passive suspension [10–12]. Moreover, an inerter can effectively improve the performance of mechanical vibration isolation systems [13–16]. To date, inertial suspension has been widely applied in train suspension [17,18], bridges [19,20], buildings [21,22], and robots [23].

With the appearance of inerters, electromechanical similarity theory has achieved a complete correspondence, where an inerter corresponds to a capacitor, a damper corresponds to a resistor, and a spring corresponds to an inductor [24]. Smith et al. improved

suspension performance by optimizing suspension layouts with an inerter in 2004 [25]. The optimization was further carried out using linear matrix inequalities, and a synthesized passive network was realized by Bott-Duffin, which indicated that the system performance could be further improved by allowing higher order passive impedance [26]. However, network synthesis for a high-order impedance can be hard to realize mechanically. Therefore, Wang et al. proposed a mechatronic inerter, consisting of a ball-screw inerter and permanent magnet electric machinery in 2011 [27], and the system impedance was realized with the combination of mechanical and electrical networks.

The research on mechatronic inerters mainly focuses in two directions. One is the mechatronic inerter [28–30] and its external circuit [31,32]. Ning et al. introduced a new controllable electrically interconnected suspension based on a mechatronic inerter in 2020, which was composed of a controllable electrical network and two independent electromagnetic suspensions [33], and the results showed that the vertical vibration and roll performance of the vehicle could be improved by controlling the resistance of the electrical network. The other direction is the simplification of higher-order impedance and synthesis of passive networks [34,35]. Shen et al. used the structure-immittance approach to implement an optimal design methodology for mechatronic ISD (inerter–spring–damper) suspension in 2022, which ensured the simplicity of the suspension structure [36]. In summary, although a mechatronic inerter can utilize an external electrical network to simulate a target mechanical impedance and improve the performance of the suspension system, the external electrical network is complex. The problem of the simplest realization of high-order impedances remains to be studied.

A bridge network is a typical electrical circuit that is widely used in electrical theory. Unlike a series-parallel network, the bridge network is a non-series-parallel network that has a special connection method; to solve the impedance expression, the equivalent conversion of the Δ structure and the Y structure is required, and the bridge network is converted into a series and parallel network and calculated [37]. Then, the simplest realization of a biquad impedance of the bridge network is realized [38]. Moreover, the impedance expressions of different bridge networks have been discussed [39], and the results indicated that a bridge network can achieve a high-order impedance, with fewer components compared with Brune synthesis. Considering the large number of high-order impedance elements and the few studies on the simplification of high-order impedance, in this paper, a bridge network is used to simplify high-order impedance and apply it to mechatronic inertial suspension. Based on electromechanical similarity theory, the electrical network of mechatronic inertial suspension is studied. In summary, the bridge network is advantageous for improving the vibration isolation performance. This paper will concentrate on the performance enhancement of a vehicle mechatronic inertial suspension system using a bridge electrical network, to make full use of the advantages of mechatronic inertial suspension.

The following parts of this paper are organized as follows: Section 2 establishes a seven-degree-of-freedom vehicle model and analyzes three bridge networks and three series-parallel networks. The parameters of the proposed bridge networks and series-parallel networks are optimized in Section 3. In Section 4, the characteristics of the bridge network (a) are simulated and analyzed, as well as compared with a series-parallel network (d). Section 5 conducts reports test of a real vehicle. Finally, the summary and conclusions are presented in Section 6.

2. Model Building

2.1. Seven-Degree-of-Freedom Vehicle Model

In order to evaluate the influence of a bridge network on the performance of a vehicle, a seven-degree-of-freedom vehicle model is established in Figure 1. The front axle suspension adopts passive suspension. As the comfort of the rear passengers is very important, this paper applies mechatronic inertial suspension to the rear suspension system, and the mechatronic inerter is connected in series with a damper and then connected in parallel

with a spring [40], as shown in Figure 1. The mechatronic inertial suspension is presented in Figure 2. The mechatronic inerter is connected to the damper in series, and the spring is connected to the mechatronic inerter and damper in parallel, when the mechatronic inerter is stimulated by vibration, the linear motion is converted into the rotating motion of the flywheel and motor through a ball screw.

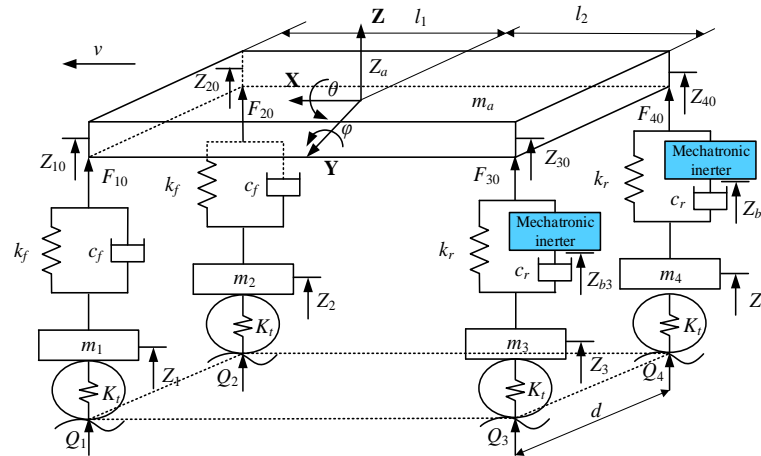


Figure 1. Seven-degree-of-freedom vehicle model.

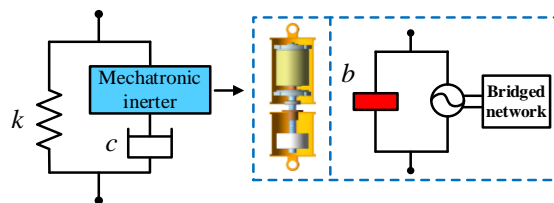


Figure 2. Mechatronic inertial suspension.

The vertical motion equation at the center of mass of the vehicle body is:

$$m_a \ddot{Z}_a = F_{10} + F_{20} + F_{30} + F_{40} \tag{1}$$

The roll motion equation of the vehicle body is:

$$I_x \ddot{\theta} = (F_{20} + F_{40} - F_{10} - F_{30}) \frac{d}{2} \tag{2}$$

The pitching motion equation of the vehicle body is:

$$I_y \ddot{\phi} = l_2 (F_{30} + F_{40}) - l_1 (F_{10} + F_{20}) \tag{3}$$

When the pitch angle and roll angle are small, the following relationship holds:

$$\begin{cases} Z_{10} = Z_a - l_1 \phi - \frac{d\theta}{2} \\ Z_{20} = Z_a - l_1 \phi + \frac{d\theta}{2} \\ Z_{30} = Z_a + l_2 \phi - \frac{d\theta}{2} \\ Z_{40} = Z_a + l_2 \phi + \frac{d\theta}{2} \end{cases} \tag{4}$$

The vertical motion equation of the unsprung mass is:

$$\begin{cases} m_1 \ddot{Z}_1 = K_t(Q_1 - Z_1) - F_{10} \\ m_2 \ddot{Z}_2 = K_t(Q_2 - Z_2) - F_{20} \\ m_3 \ddot{Z}_3 = K_t(Q_3 - Z_3) - F_{30} \\ m_4 \ddot{Z}_4 = K_t(Q_4 - Z_4) - F_{40} \end{cases} \quad (5)$$

The forces of the four suspensions are:

$$\begin{cases} F_{10} = k_f(Z_1 - Z_{10}) + c_f(\dot{Z}_1 - \dot{Z}_{10}) \\ F_{20} = k_f(Z_2 - Z_{20}) + c_f(\dot{Z}_2 - \dot{Z}_{20}) \\ F_{30} = k_r(Z_3 - Z_{30}) + u_3 \\ u_3 = b(\ddot{Z}_{b3} - \ddot{Z}_{30}) + \left(\frac{2\pi}{P}\right)^2 \frac{k_t k_e}{Z} (\dot{Z}_{b3} - \dot{Z}_{30}) = c_r(\dot{Z}_3 - \dot{Z}_{b3}) \\ F_{40} = k_r(Z_4 - Z_{40}) + u_4 \\ u_4 = b(\ddot{Z}_{b4} - \ddot{Z}_{40}) + \left(\frac{2\pi}{P}\right)^2 \frac{k_t k_e}{Z} (\dot{Z}_{b4} - \dot{Z}_{40}) = c_r(\dot{Z}_4 - \dot{Z}_{b4}) \end{cases} \quad (6)$$

where m_a is the sprung mass. m_1 , m_2 , m_3 , and m_4 are the unsprung mass of the four suspensions, respectively. K_t is the equivalent stiffness of the tire. k_f and c_f are the spring stiffness and the damping coefficient of the front suspensions, respectively. k_r and c_r are the spring stiffness and the damping coefficient of rear suspensions, respectively. Z_{10} , Z_{20} , Z_{30} , and Z_{40} are the vertical displacements of the connection between the vehicle body and the four suspensions. F_{10} , F_{20} , F_{30} , and F_{40} are the forces of the four suspensions, respectively. Z_1 , Z_2 , Z_3 , and Z_4 are the vertical displacements of four unsprung masses, respectively. Z_{b3} and Z_{b4} are the vertical displacements of the mechatronic inerter of the left rear suspension and the right rear suspension. Q_1 , Q_2 , Q_3 , and Q_4 are the displacement inputs of the four wheels. Z_a is the vertical displacement of the sprung mass. θ is the body roll angle, and I_x is the body roll moment of inertia. φ is the body pitch angle, and I_y is the body pitch moment of inertia. l_1 and l_2 are the distance from the front axle and rear axle to the body centroid, respectively. d is the wheelbase, b is the inertial coefficient of the mechatronic inerter, and v is the vehicle speed. k_t and k_e are the inductive torque constant and the inductive voltage constant of the rotating motor, respectively. Z is the impedance of the external circuit of the rotating motor. u_3 and u_4 are the forces of the series branch of the mechatronic inerter and the damper, respectively. P is the lead of the ball screw.

In this paper, a real vehicle was used for the test, the simulation parameters refer to real vehicle data, and the main dimensional parameters of the vehicle were obtained according to the vehicle user manual, as shown in Table 1.

Table 1. Main parameters of the vehicle model.

Parameters	Symbol	Unit	Value
Sprung mass	m_a	kg	1659
Unsprung mass of left and right front wheels	m_1, m_2	kg	47.5
Unsprung mass of left and right rear wheels	m_3, m_4	kg	42.5
Spring stiffness of front axle suspension	k_f	kN·m ⁻¹	25
Spring stiffness of rear axle suspension	k_r	kN·m ⁻¹	22
Damping coefficient of front axle suspension	c_f	kN·s·m ⁻¹	1.8
Damping coefficient of rear axle suspension	c_r	kN·s·m ⁻¹	1.5
Equivalent stiffness of tire	K_t	kN·m ⁻¹	192
Distance from front axle to body centroid	l_1	m	1.28
Distance from rear axle to body centroid	l_2	m	1.43
Wheelbase	d	m	1.62
Inertance of rear suspension	b	kg	308
Body roll moment of inertia	I_x	kg·m ²	1088
Body pitch moment of inertia	I_y	kg·m ²	3032

2.2. Bridge Network

Common bridge networks include a bridge rectifier circuit, half bridge circuit, full bridge circuit, wheatstone bridge, balanced bridge, and unbalanced bridge. The bridge network used in this paper was an unbalanced bridge circuit. The most common bridge network consists of five resistance elements, as shown in Figure 3a. And Figure 3b is the equivalent network.

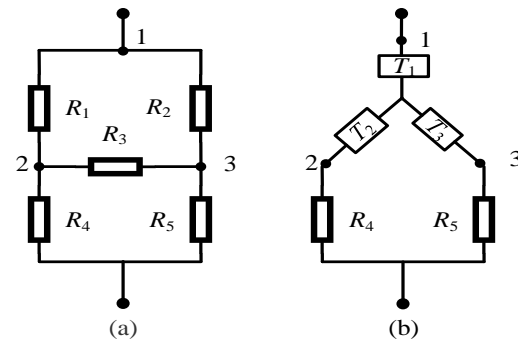


Figure 3. (a). bridge network consists of five resistance elements. (b). Equivalent network of the bridge network.

Where $R_1, R_2, R_3, R_4,$ and R_5 are resistors, $T_1, T_2,$ and T_3 are equivalent impedances.

In Figure 3, when the Δ structure of Figure 3a is transformed into the Y structure of Figure 3b, the equivalent transformation equation is:

$$\begin{cases} T_1 = \frac{R_1 R_2}{R_1 + R_2 + R_3} \\ T_2 = \frac{R_1 R_3}{R_1 + R_2 + R_3} \\ T_3 = \frac{R_2 R_3}{R_1 + R_2 + R_3} \end{cases} \quad (7)$$

Therefore, the impedance expression of Figure 3a is:

$$Z = T_1 + \frac{(T_2 + R_4)(T_3 + R_5)}{T_2 + R_4 + T_3 + R_5} \quad (8)$$

A bridge network composed of resistance, capacitance, and inductance has many kinds of structures. In this paper, the three most basic bridge networks are selected. Considering the special solution method of a bridge network, the selection principles of the bridge network studied in this paper were as follows. First of all, a resistor, a capacitor, and an inductor can constitute three kinds of Δ structures and three kinds of Y structures, respectively. Since the impedance of the resistance has no effect on the total impedance order [41], the remaining two elements of the bridge network are selected as resistors to form a five-element bridge network with three resistors, one capacitor, and one inductor, as shown in Figure 4.

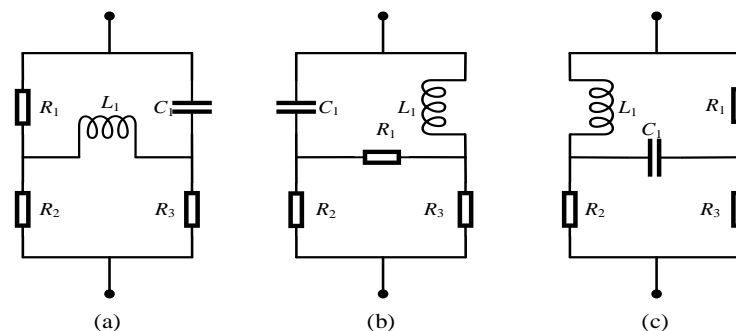


Figure 4. (a–c) are five-element bridge networks of three different structures.

According to the impedance transformation method shown in the Equation (8), the impedance transfer function of Figure 4a can be expressed as:

$$\frac{1}{Z_a(s)} = \frac{A_1s^4 + B_1s^3 + C_1s^2 + D_1s + E_1}{F_1s^4 + G_1s^3 + H_1s^2 + I_1s + J_1} \quad (9)$$

$$\begin{aligned} A_1 &= (R_1 + R_2 + R_3)L_1^2C_1^2, \\ B_1 &= (R_1R_2C_1 + R_1R_3C_1 + L_1)L_1C_1 + (R_1 + R_2 + R_3)R_1L_1C_1^2, \\ C_1 &= (R_1R_2C_1 + R_1R_3C_1 + L_1)R_1C_1 + (R_1 + 2R_2 + 2R_3)L_1C_1, \\ D_1 &= 2R_1C_1(R_2 + R_3) + L_1, \\ E_1 &= R_2 + R_3, \\ F_1 &= (R_1 + R_2)R_3L_1^2C_1^2, \\ G_1 &= (R_1 + R_2)(R_1R_3C_1 + L_1)L_1C_1 + R_1R_2R_3L_1C_1^2, \\ H_1 &= (R_1 + R_2 + R_3)R_1L_1C_1 + (R_1 + R_2)R_3L_1C_1 + (R_1R_3C_1 + L_1)R_1R_2C_1 + R_2R_3L_1C_1, \\ I_1 &= (R_1R_2C_1 + R_1R_3C_1 + L_1)R_1 + R_1R_2R_3C_1 + (R_1R_3C_1 + L_1)R_2, \\ J_1 &= (R_2 + R_3)R_1 + R_2R_3. \end{aligned} \quad (10)$$

Similarly, it was calculated that the orders of the impedance transfer functions of the bridge network (b) and the bridge network (c) were also double fourth order, which will not be repeated here.

2.3. Series-Parallel Network

Correspondingly, three five-element series-parallel networks are shown in Figure 5.

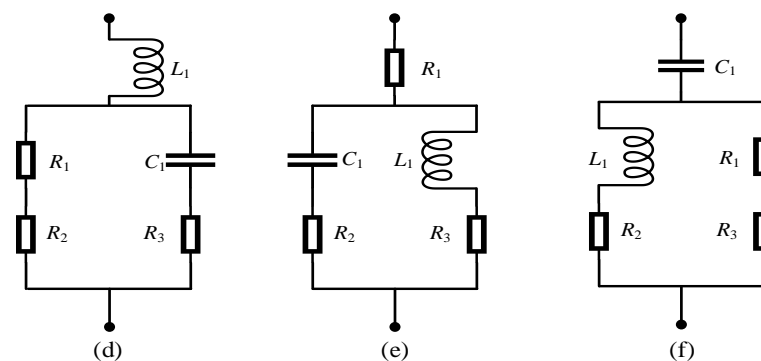


Figure 5. (d–f) are five-element series-parallel networks of three different structures.

From electrical knowledge, the impedances of the three series-parallel networks in Figure 5d–f were all of biquadratic order. With the same number of components, the bridge network can achieve a higher order impedance than the series-parallel network.

3. Optimization of the Inertial Suspension Parameters

In order to achieve the best performance of the mechatronic inertial suspension, the parameters of the suspension needed to be optimized. In this paper, the particle swarm optimization (PSO) algorithm, which is suitable for multi-objective environments, was selected to optimize the structural parameters of the external electric circuit of the mechatronic inerter. The PSO algorithm is an intelligent optimization algorithm, whose basic idea is to initialize a group of random particles (random solutions) and find the optimal solution through iteration. The specific optimization process is shown in the Figure 6. To begin, the particle is initialized, the fit value of the particle is then compared with the best location it passes through, and the speed and position of the particle is updated. The process ends when the termination condition is met in each iteration, the particles update their position attributes by tracking the individual extremum and global extremum, and finally find the optimal particle [42]. The PSO algorithm has the advantages of fast search speed and memory, due to the need to adjust few parameters, so the structure

is simple, and it is suitable for solving practical engineering problems. Particle velocities and positions are updated in accordance with the following two formulas:

$$V^{k+1} = \lambda V^k + d_1 r_1 (P_{id}^k - X^k) + d_2 r_2 (P_{gd}^k - X^k) \quad (11)$$

$$X^{k+1} = X^k + V^{k+1} \quad (12)$$

where λ is the inertia factor, its value affects the global and individual optimization ability. V is the velocity of the particle. X is the current position of the particle, and k is the current number of iterations. d_1 and d_2 are non-negative constants, called acceleration factors, and the general range is between 0 and 4. r_1 and r_2 are random numbers between (0, 1). P_{id} and P_{gd} are the individual extremum and global extremum, respectively.

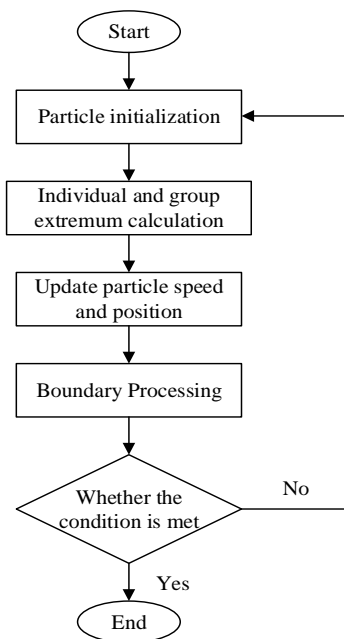


Figure 6. Parameter optimization flow chart.

This paper mainly studies the influence of the bridge network and the series-parallel network on the mechatronic inertial suspension, so three resistors (R_1, R_2, R_3), one capacitor (C_1), and one inductor (L_1) of the external electrical circuit are taken as individuals to be solved. Moreover, the performance indicators have different units and orders of magnitude, so it is necessary to establish a unified objective function. The performance indexes of the mechatronic inertial suspension are divided by the corresponding indexes of the passive suspension, and the sum of their quotients is taken as the objective function. In this paper, f is the objective function of optimization, which is obtained by weighting the following parameters. The influence of different units of evaluation indexes is ignored; meanwhile, the improvement of suspension performance is studied by quantifying the objective function. Therefore, the optimization of evaluation indexes of the ride comfort and the road friendliness is transformed into the minimum value problem of the unified objective function. The smaller the value of the optimization objective function, the better the optimization effect, and the performance improvement is obvious. In the optimization process, the road condition and running speed are set as C grade and 20 km/h, respectively, and the number of iterations is 100. Due to the mechatronic inertial suspension being used to replace the rear suspension system, the relevant evaluation indexes of the rear

suspension are mainly used as the optimization objectives. The expression of the unified objective function and constraint conditions are as follows:

$$f = \frac{BA(P)}{BA_{pas}} + \frac{LRSWS(P)}{LRSWS_{pas}} + \frac{LRDTL(P)}{LRDTL_{pas}} + \frac{RRSWS(P)}{RRSWS_{pas}} + \frac{RRDTL(P)}{RRDTL_{pas}} \tag{13}$$

$$P = [C_1 \quad L_1 \quad R_1 \quad R_2 \quad R_3] \tag{14}$$

$$s.t. \begin{cases} BA(P) < BA_{pass} \\ LRSWS(P) < LRSWS_{pas} \\ LRDTL(P) < LRDTL_{pass} \\ RRSWS(P) < RRSWS_{pas} \\ RRDTL(P) < RRDTL_{pass} \\ LM < P < UM \end{cases} \tag{15}$$

$$\begin{aligned} LM &= [0, 0, 0, 0, 0] \\ UM &= [10, 100, 5000, 5000, 5000] \end{aligned} \tag{16}$$

where $BA(P)$, $LRSWS(P)$, $LRDTL(P)$, $RRSWS(P)$, and $RRDTL(P)$ indicate the root mean square (RMS) of the centroid acceleration, working space of the left rear wheel suspension, dynamic tire load of the left rear wheel, working space of the right rear wheel suspension, and dynamic tire load of the right rear wheel of the optimized mechatronic inertial suspension, respectively. The above parameters were used to evaluate the ride comfort and road friendliness of the vehicle. BA_{pas} , $LRSWS_{pas}$, $LRDTL_{pas}$, $RRSWS_{pas}$, and $RRDTL_{pas}$ are the RMS of the corresponding performance indexes of the traditional passive suspension. P is the set of parameters to be optimized. LM and UM are the upper and lower bounds of these parameters, and these parameters will affect the handling stability of the vehicle.

After many iterations, the optimized parameters of the proposed bridge network and series-parallel network were revealed, as shown in Table 2.

Table 2. Optimized parameters of the electrical network.

Parameters	Bridge Network			Series-Parallel Network		
	(a)	(b)	(c)	(d)	(e)	(f)
Capacitance C_1 (mF)	8	3	8.4	6.3	2.5	7.5
Inductance L_1 (mH)	18.8	17.5	3.5	16	13.7	15
Resistance R_1 (Ω)	2908	2553	857	2976	2856	2598
Resistance R_2 (Ω)	2984	2824	3000	2768	2708	2714
Resistance R_3 (Ω)	2992	2996	1350	2748	2158	2944

4. Discussion

In this section, numerical simulations are carried out to verify the effectiveness of the mechatronic inertial suspension based on the bridge network (a).

4.1. Road Input

Assuming the vehicle is driving at a speed of u on a grade C road, the random road input is expressed as:

$$\dot{z}_r(t) = -0.111[uz_r(t) + 40\sqrt{G_q(n_0)}uw(t)] \tag{17}$$

where $z_r(t)$ is the vertical displacement of the random road input, $w(t)$ is the white noise with mean value of 0, and $G_q(n_0)$ is the road roughness ($2.56/10^4 \text{ m}^3$).

In the simulation model, four road inputs were required. The random road input of the left front wheel is the same as that of the left rear wheel, but the random road inputs of left front wheel and right front wheel are slightly different. In addition, the time when the

front wheel and the rear wheel receive the road input is different in the simulation process. Therefore, the wheelbase divided by the speed was the value of the delay in the simulation, and the left rear wheel and the right rear wheel have a delay compared with the left front wheel and the right front wheel, respectively.

In this paper, the road inputs of the left front wheel and the right front wheel are almost the same; thus, those of the left rear wheel and the right rear wheel are also virtually identical. To make this paper concise and clear, the centroid acceleration, vehicle body pitch angular acceleration, vehicle body roll angular acceleration, working spaces of the left front wheel suspension and the left rear wheel suspension, and the dynamic tire loads of the left front wheel and the left rear wheel were selected as the performance evaluation indexes.

4.2. Performance Analysis of Mechatronic Inertial Suspension

The parameters in Tables 1 and 2 were input into the proposed mechatronic inertial suspension based on a bridge electrical network and a series-parallel electrical network for simulation. The vehicle speed was 20 m/s. The RMS values of performance indexes were obtained, as shown in Tables 3 and 4.

Table 3. RMS comparison of mechatronic inertial suspension based on the bridge network.

Suspension Performance Index	Passive Suspension	Bridge Network		
		(a)	(b)	(c)
RMS of centroid acceleration ($\text{m}\cdot\text{s}^{-2}$)	1.8792	1.7902	1.8023	1.8010
RMS of body roll angular acceleration ($\text{rad}\cdot\text{s}^{-2}$)	0.1059	0.1044	0.1037	0.1037
RMS of body pitch angular acceleration ($\text{rad}\cdot\text{s}^{-2}$)	1.3827	1.3440	1.3532	1.3539
RMS of working space of left front suspension (m)	0.0266	0.0256	0.0257	0.0257
RMS of dynamic tire load of left front wheel (kN)	1.9287	1.8665	1.8781	1.8781
RMS of working space of left rear suspension (m)	0.0271	0.0201	0.0202	0.0203
RMS of dynamic tire load of left rear wheel (kN)	1.8907	1.7389	1.7497	1.7495

Table 4. RMS comparison of mechatronic inertial suspension based on the series-parallel network.

Suspension Performance Index	Passive Suspension	Series-Parallel Network		
		(d)	(e)	(f)
RMS of centroid acceleration ($\text{m}\cdot\text{s}^{-2}$)	1.8792	1.8354	1.8378	1.8446
RMS of body roll angular acceleration ($\text{rad}\cdot\text{s}^{-2}$)	0.1059	0.1131	0.1125	0.1125
RMS of body pitch angular acceleration ($\text{rad}\cdot\text{s}^{-2}$)	1.3827	1.4571	1.4591	1.4642
RMS of working space of left front suspension (m)	0.0266	0.0253	0.0252	0.0254
RMS of dynamic tire load of left front wheel (kN)	1.9287	1.8444	1.8441	1.8528
RMS of working space of left rear suspension (m)	0.0271	0.0229	0.0233	0.0230
RMS of dynamic tire load of left rear wheel (kN)	1.8907	1.7855	1.7897	1.7935

From Tables 3 and 4, it can be noted that among three mechatronic inertial suspensions based on the bridge network, the bridge network (a) had the best improvement in vehicle performance. Similarly, the series-parallel network (d) was the best in its group. Moreover, compared with the series-parallel network (d), the mechatronic inertial suspension based on the bridge network (a) had a greater effect on improving the performance of the vehicle. According to Section 2, it can be concluded that with the same number of electrical components, the bridge network could achieve a higher order impedance compared with the series-parallel network. Therefore, the bridge network (a) was selected as the external electrical network for the mechatronic inerter for the following part.

5. Experimental Research

To further validate the vibration isolation performance of the vehicle mechatronic inertial suspension system employing a bridge electrical network (a), a test of a real vehicle was carried out on the road.

5.1. Structure Selection and Real Vehicle Installation

The key components of mechatronic inerter include the ball–screw pair, flywheel, and rotating motor. The specific parameters were determined, as shown in Table 5.

Table 5. Parameters of the key components.

Parameter	Value	Parameter	Value
Nominal shaft diameter d_0 (mm)	16	Rated power P (W)	2000
Lead P (mm)	5	Rated speed n_e (r·min ⁻¹)	3000
Center distance of balls on both sides d_p (mm)	16.75	Maximum speed n_m (r·min ⁻¹)	6000
Groove diameter d_c (mm)	13.5	Rated torque T_e (N·m)	5.88
Number of columns × Number of turns	1 × 2.65	Rated voltage U_e (V)	310
Effective stroke l_0 (mm)	120	Rated current I_e (A)	6
Lead screw stiffness k_t (N·μm ⁻¹)	130	Inductive torque constant k_t (N·m/A)	0.98
Dynamic rated load c_a (kN)	5.4	Inductive voltage constant k_e (V·s/rad)	0.98
Static rated load c_{0a} (kN)	13.3	Allowable stress σ_p (N·mm ⁻²)	150
Dynamic load coefficient k_s	2	Radius of flywheel r (mm)	30
Static load coefficient k_d	3	Thickness of flywheel h (mm)	20

After completing the parameter design of the ball–screw pair, flywheel, and rotating motor, a mechatronic inerter based on a bridge network (a) was developed and connected in series with the damper. Then they were installed in the rear suspension of the test vehicle, to prepare for the subsequent road test, to comprehensively analyze the performance advantages of a mechatronic inertial suspension based on a bridge network (a). In addition, three axis acceleration sensors, a PCB acceleration sensor, a SICK laser displacement sensor, and Siemens LMS Test Lab data acquisition instrument were used to collect the centroid acceleration, roll angular acceleration, pitch angular acceleration, suspension working space, and dynamic tire load signals of the test vehicle.

The test instruments and real vehicle test are shown in Figure 7.

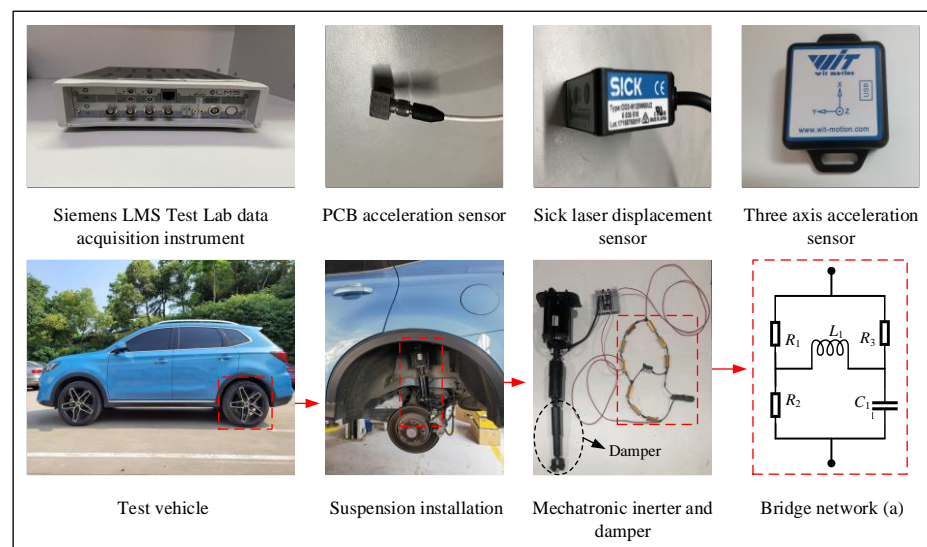


Figure 7. Test instruments and real vehicle test.

5.2. Random Road Input

It was assumed that the test vehicle ran at a speed of 20 km/h on a C grade road. To ensure the consistency of the random road input, the test vehicle was tested on the same road section and ran along the white solid line of the road. The sampling interval was 0.005 s, and the sampling time was 10 s. The result of time domain is shown in Figure 8 and Table 6.

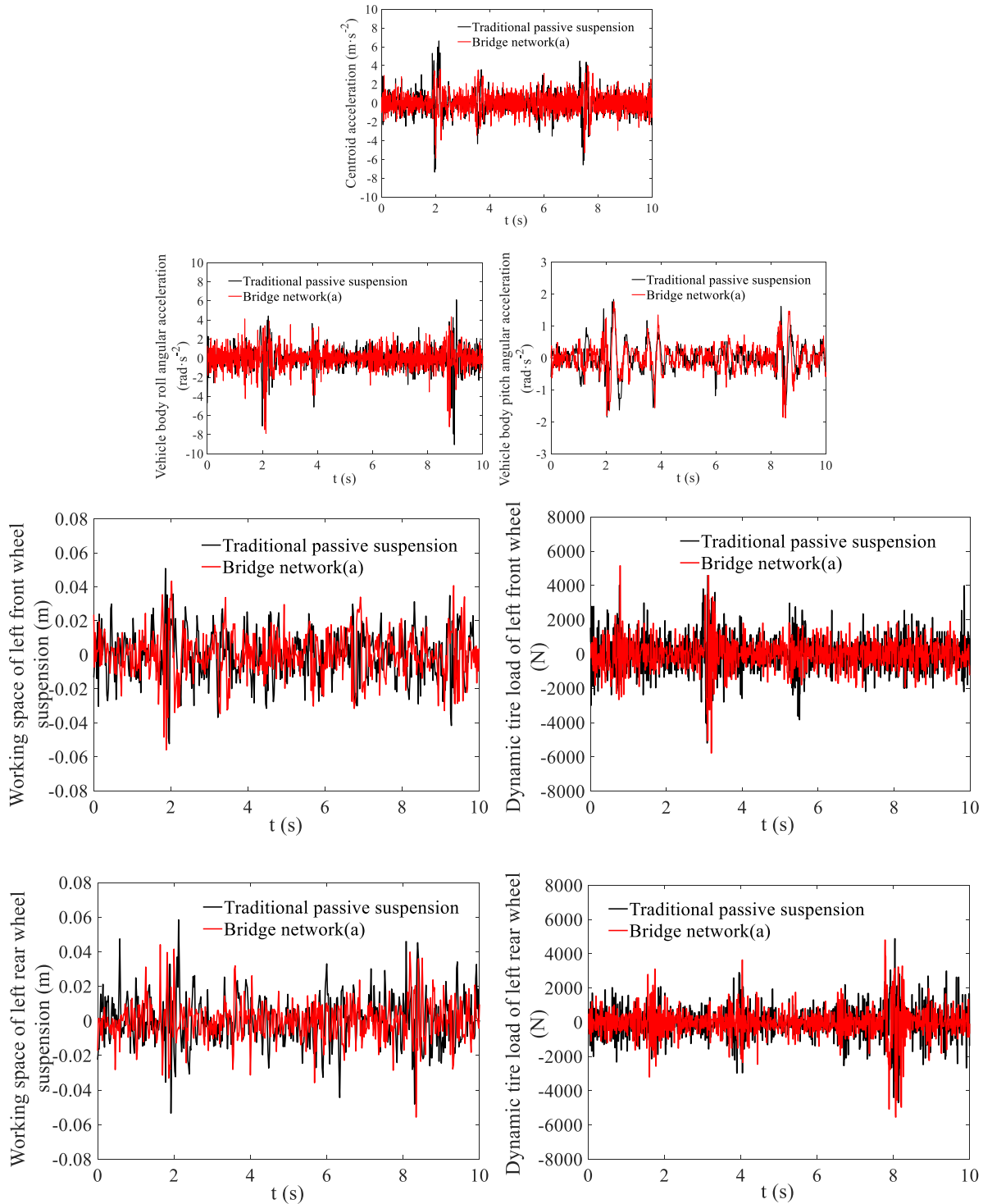


Figure 8. Performance comparison under random road conditions with a vehicle speed of 20 km/h.

Table 6. Performance index with a random input.

Performance Index	RMS of Passive Suspension	RMS	Bridge Network (a) Improvement (%)
Centroid acceleration ($\text{m}\cdot\text{s}^{-2}$)	1.2656	1.2428	1.8
Vehicle body roll angular acceleration ($\text{rad}\cdot\text{s}^{-2}$)	1.1139	1.0526	5.5
Vehicle body pitch angular acceleration ($\text{rad}\cdot\text{s}^{-2}$)	0.4426	0.4643	-4.9
Working space of left front suspension (m)	0.0142	0.0138	2.5
Dynamic tire load of left front wheel (N)	1022	1000	2.2
Working space of left rear suspension (m)	0.0145	0.0114	21.1
Dynamic tire load of left rear wheel (N)	981	919	6.3

It can be seen from Table 6 and Figure 8 that, compared with the passive suspension, the RMS values of centroid acceleration and vehicle body roll angular acceleration of the mechatronic inertial suspension based on a bridge network (a) were reduced by 1.8% and 5.5%, respectively. While, the RMS values of the suspension working space and dynamic tire load of the left rear suspension, comparing the passive suspension with the mechatronic inertial suspension based on a bridge network (a), were decreased by 21.1% and 6.3%. The above improvements improved the ride comfort of the vehicle. However, the RMS value of vehicle body pitch angular acceleration was increased by 4.9%, and this increase of vehicle body pitch angular acceleration made vehicle handling stability slightly worse. Meanwhile, considering that only the rear suspension system adopted the proposed mechatronic inertial suspension based on a bridge network, it was found that the RMS values of the suspension working space and dynamic tire load of the left front suspension were improved by 2.5% and 2.2%, respectively, which is less than the improvement effect of the rear suspension system. It can be concluded from the above results that the bridge network (a) could improve the ride comfort of the vehicle, but the effect was not sufficiently significant, and the handling stability was not improved.

5.3. Pulse Road Input

A comparison of the peak value of performance indexes with a pulse road input and when the vehicle speed was 20 km/h is shown in Table 7 and Figure 9.

Table 7. Performance index with a pulse road input.

Performance Index	Peak to Peak of Passive Suspension	Peak to Peak	Bridge Network (a) Improvement (%)
Centroid acceleration ($\text{m}\cdot\text{s}^{-2}$)	7.2110	7.1722	0.5
Vehicle body roll angular acceleration ($\text{rad}\cdot\text{s}^{-2}$)	4.9686	4.5532	8.4
Vehicle body pitch angular acceleration ($\text{rad}\cdot\text{s}^{-2}$)	9.6225	10.1903	-5.9
Working space of left front suspension (m)	0.1128	0.1102	2.3
Dynamic tire load of left front wheel (N)	7200	7038	2.2
Working space of left rear suspension (m)	0.1234	0.1008	18.3
Dynamic tire load of left rear wheel (N)	7047	6568	6.8

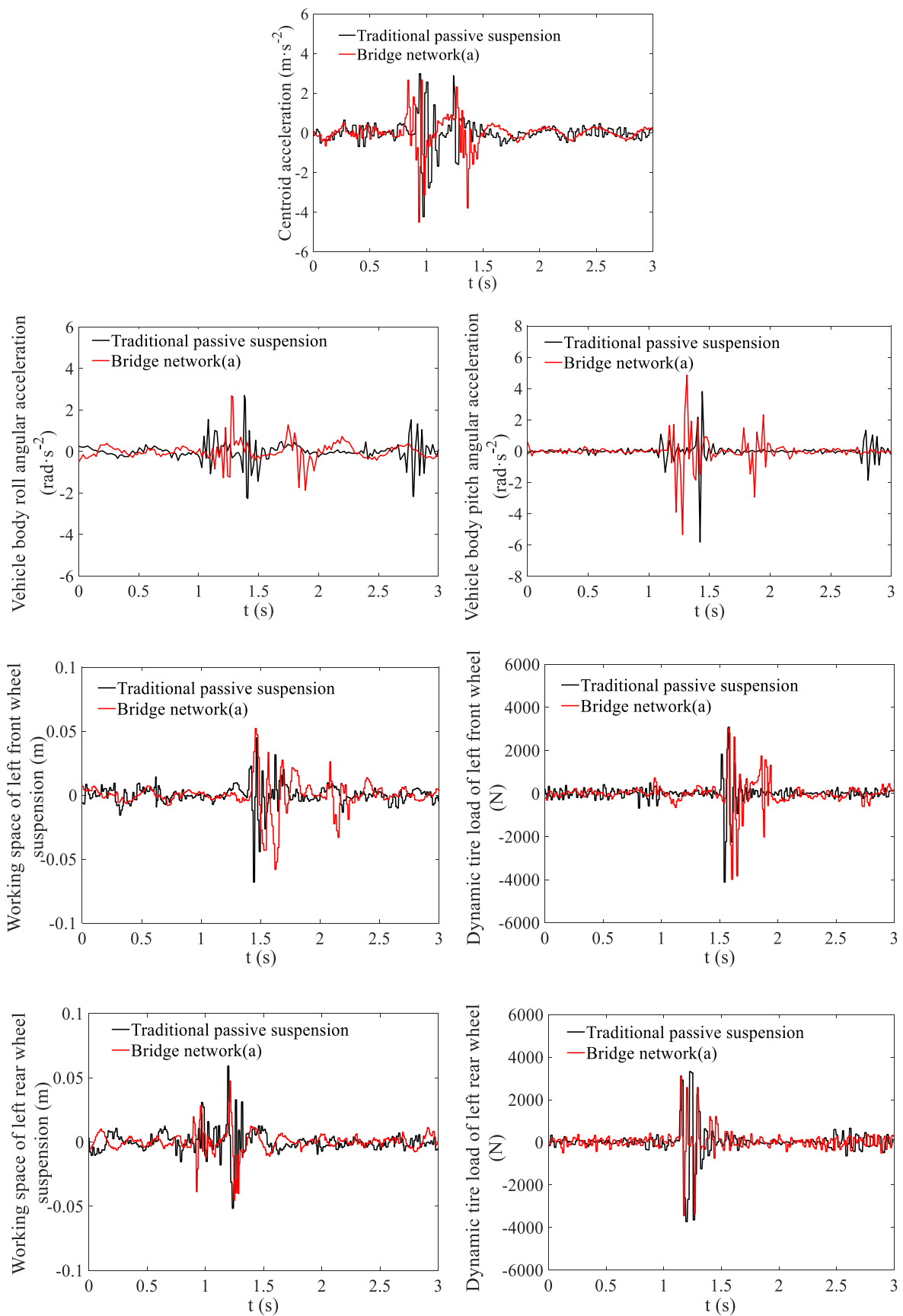


Figure 9. Comparison diagram with a pulse road input with a vehicle speed of 20 km/h.

From Table 7 and Figure 9, we can see that, for the centroid acceleration, the improvement of the peak to peak of the mechatronic inertial suspension based on the bridge network (a) was much smaller than that of the passive suspension, from $7.2110 \text{ (m}\cdot\text{s}^{-2}\text{)}$ to $7.1722 \text{ (m}\cdot\text{s}^{-2}\text{)}$, which is only 0.5% and helped to improve the vehicle ride comfort. However, for the vehicle body roll angular acceleration, the improvement was apparent, from $4.9686 \text{ (rad}\cdot\text{s}^{-2}\text{)}$ to $4.5532 \text{ (rad}\cdot\text{s}^{-2}\text{)}$, and the degree of reduction was 8.4%. For the vehicle body pitch angular acceleration, the peak to peak of the mechatronic inertial suspension was relatively higher than that of the passive suspension, which increased from $9.6225 \text{ (rad}\cdot\text{s}^{-2}\text{)}$ to $10.1903 \text{ (rad}\cdot\text{s}^{-2}\text{)}$ (5.9%), and there was no improvement in the vehicle handling stability. The peak to peak values of the suspension working space and dynamic tire load of the left front suspension, comparing the passive suspension with the mechatronic inertial suspension based on a bridge network (a), were reduced by 2.3% and 2.2%, respectively. The performance improvement of the left rear suspension was obvious compared to the left front suspension. The suspension working space decreased from 0.1234 (m) to 0.1008 (m) (18.3%), and the dynamic tire load decreased from 7047 (N) to 6568 (N) (6.8%). These improvements helped to improve the vehicle ride comfort and road friendliness.

In summary, the proposed mechatronic inertial suspension based on a bridge network (a) can better realize a high-order suspension impedance and has better working performance, to effectively improve the ride comfort and vibration isolation performance of vehicles.

6. Conclusions

In this paper, the optimal design of mechatronic inertial suspension with an external electrical network was studied. First, an optimization design method of the external circuit of vehicle mechatronic inertial suspension was proposed using a bridge network. Then, a whole-vehicle dynamic model, considering the vertical motion, roll motion, and pitch motion of vehicle body, was established, and the basic structure and impedance transfer function of the bridge network and series-parallel network were analyzed. The particle swarm optimization algorithm was used to optimize component parameters of three bridge networks and three series-parallel networks. Then, a performance comparison and analysis of the mechatronic inertial suspension using a bridge network and series-parallel network was studied, and the bridge network (a) and series-parallel network (d) were selected. On this basis, the bridge network (a) and series-parallel network (d) were compared in the time domain and frequency domain, and the bridge network (a) with better vibration suppression ability was selected as the electrical network for the mechatronic inerter. Finally, a road test with a real vehicle was carried out with a random road input and pulse road input, respectively.

The results show that, under the random input condition, compared with the passive suspension, the mechatronic inertial suspension based on a bridge network (a) could reduce the RMS value of centroid acceleration by 1.8%, the RMS value of the body roll angular acceleration by 5.5%, and the RMS values of the suspension working space and dynamic tire load of the left rear wheel suspension by 21.1% and 6.3%, respectively, which effectively improved the ride comfort of the vehicle.

This article provides a research direction for the passive optimization design of mechatronic inertial suspension and verified its effectiveness and feasibility, laying the foundation for further improvements of the vibration isolation of vehicle mechatronic inertial suspension.

Author Contributions: Conceptualization, X.Y.; methodology, Y.S.; software, T.Z.; validation, X.L.; formal analysis, T.H.; investigation, T.H.; writing—original draft preparation, T.Z.; writing—review and editing, Y.S.; supervision, X.Y. All authors have read and agreed to the published version of the manuscript.

Funding: The authors disclose receipt of the following financial support for the research, authorship, and/or publication of this article: This research was funded by the National Natural Science

Foundation of China under Grant 52072157 and 52002156, the Natural Science Foundation of Jiangsu Province under Grant BK20200911 and Natural Science Foundation of Beijing Municipality under Grant 3214045.

Data Availability Statement: Not applicable.

Acknowledgments: The authors would like to thank the editor and the anonymous reviewers for their careful reading and helpful comments.

Conflicts of Interest: No potential conflict of interest are reported by the authors.

References

1. Lee, D.; Jin, S.W.; Rhee, E.-J.; Lee, C. Practical Damper Velocity Estimation for Semi-Active Suspension Control. *Int. J. Automot. Technol.* **2021**, *22*, 499–506. [[CrossRef](#)]
2. Lee, G.-W.; Hyun, M.; Kang, D.-O.; Heo, S.-J. High-efficiency Active Suspension based on Continuous Damping Control. *Int. J. Automot. Technol.* **2022**, *23*, 31–40. [[CrossRef](#)]
3. Smith, M. Synthesis of mechanical networks: The inerter. *IEEE Trans. Autom. Control* **2002**, *47*, 1648–1662. [[CrossRef](#)]
4. Papageorgiou, C.; Houghton, N.E.; Smith, M.C. Experimental testing and analysis of inerter devices. *J. Dyn. Syst. Meas. Control.-Trans. Asme* **2009**, *131*, 101–116. [[CrossRef](#)]
5. Faraj, R.; Jankowski, L.; Graczykowski, C.; Holnicki-Szulc, J. Can the inerter be a successful shock-absorber? The case of a ball-screw inerter with a variable thread lead. *J. Frankl. Inst.* **2019**, *356*, 7855–7872. [[CrossRef](#)]
6. Liu, X.; Jiang, J.Z.; Titurus, B.; Harrison, A. Model identification methodology for fluid-based inerters. *Mech. Syst. Signal Process.* **2018**, *106*, 479–494. [[CrossRef](#)]
7. Swift, S.J.; Smith, M.C.; Glover, A.R.; Papageorgiosu, C.; Gartner, B.; Houghton, N.E. Design and modelling of a fluid inerter. *Int. J. Control.* **2013**, *86*, 2035–2051. [[CrossRef](#)]
8. Shen, Y.; Chen, L.; Liu, Y.; Zhang, X. Modeling and Optimization of Vehicle Suspension Employing a Nonlinear Fluid Inerter. *Shock Vib.* **2016**, *2016*, 1–9. [[CrossRef](#)]
9. Zhang, H.; Shen, Y.; Yang, H. Impact of coil factors on a hydraulic electric inerter based vehicle suspension. *J. Theor. Appl. Mech.* **2020**, *58*, 711–722. [[CrossRef](#)]
10. Yang, X.; Song, H.; Shen, Y.; Liu, Y.; He, T. Control of the Vehicle Inertial Suspension Based on the Mixed Skyhook and Power-Driven-Damper Strategy. *IEEE Access* **2020**, *8*, 217473–217482. [[CrossRef](#)]
11. Li, X.; Li, F.; Shang, D. Dynamic Characteristics Analysis of ISD Suspension System under Different Working Conditions. *Mathematics* **2021**, *9*, 1345. [[CrossRef](#)]
12. Zhao, Z.; Zhang, R.; Wierschem, N.E.; Jiang, Y.; Pan, C. Displacement mitigation-oriented design and mechanism for inerter-based isolation system. *J. Vib. Control.* **2021**, *27*, 1991–2003. [[CrossRef](#)]
13. Shi, A.; Shen, Y.; Wang, J. Parameter optimization of a grounded dynamic vibration absorber with lever and inerter. *J. Low Freq. Noise, Vib. Act. Control* **2022**, *41*, 784–798. [[CrossRef](#)]
14. Zhang, R.F.; Zhao, Z.P.; Liu, X.C.; Zhang, L.X. Optimal design of inerter systems for the force-transmission suppression of oscillating structures. *Earthq. Eng. Eng. Vib.* **2022**, *21*, 441–454.
15. Dai, J.; Wang, Y.; Wei, M.; Zhang, W.; Zhu, J.; Jin, H.; Jiang, C. Dynamic characteristic analysis of the inerter-based piecewise vibration isolator under base excitation. *Acta Mech.* **2022**, *233*, 513–533. [[CrossRef](#)]
16. Lewis, T.D.; Jiang, J.Z.; Neild, S.A.; Gong, C.N.; Iwnicki, S.D. Using an inerter-based suspension to improve both passenger comfort and track wear in railway vehicles. *Veh. Syst. Dyn.* **2020**, *58*, 472–493. [[CrossRef](#)]
17. Xia, Z.H.; Zhou, J.S.; Lian, J.Y.; Ding, S.; Gong, D.; Sun, W.; Sun, Y. Online detection and control of car body low-frequency swaying in railway vehicles. *Veh. Syst. Dyn.* **2021**, *59*, 70–100. [[CrossRef](#)]
18. Wang, Y.; Li, H.X.; Meng, H.D.; Wang, Y. Dynamic characteristics of an underframe inerter-based suspended equipment for high speed trains. *J. Vib. Shock.* **2022**, *41*, 246–254.
19. Zhang, H.; Ye, Z.; Chen, X.; Yao, W. Seismic response mitigation of girder displacement of cable-stayed bridge using inerter systems. *Structures* **2022**, *39*, 928–944. [[CrossRef](#)]
20. Xu, K.; Bi, K.; Han, Q.; Li, X.; Du, X. Using tuned mass damper inerter to mitigate vortex-induced vibration of long-span bridges: Analytical study. *Eng. Struct.* **2019**, *182*, 101–111. [[CrossRef](#)]
21. Zhao, Z.; Chen, Q.; Zhang, R.; Jiang, Y.; Pan, C. A negative stiffness inerter system (NSIS) for earthquake protection purposes. *Smart Struct. Syst.* **2020**, *26*, 481–493.
22. Li, Y.; Li, S.; Chen, Z. Optimal design and effectiveness evaluation for inerter-based devices on mitigating seismic responses of base isolated structures. *Earthq. Eng. Eng. Vib.* **2021**, *20*, 1021–1032. [[CrossRef](#)]
23. Xu, S.; He, B. A compliance modeling method of flexible rotary joint for collaborative robot using passive network synthesis theory. *Proc. Inst. Mech. Eng. Part C J. Mech. Eng. Sci.* **2021**, *236*, 4038–4048. [[CrossRef](#)]
24. Yang, X.; He, T.; Shen, Y.; Liu, Y.; Yan, L. Research on predictive coordinated control of ride comfort and road friendliness for heavy vehicle ISD suspension based on the hybrid-hook damping strategy. *Proc. Inst. Mech. Eng. Part D J. Automob. Eng.* **2022**. [[CrossRef](#)]

25. Smith, M.C.; Wang, F.-C. Performance Benefits in Passive Vehicle Suspensions Employing Inerters. *Veh. Syst. Dyn.* **2004**, *42*, 235–257. [[CrossRef](#)]
26. Papageorgiou, C.; Smith, M. Positive real synthesis using matrix inequalities for mechanical networks: Application to vehicle suspension. *IEEE Trans. Control Syst. Technol.* **2006**, *14*, 423–435. [[CrossRef](#)]
27. Wang, F.-C.; Chan, H.-A. Vehicle suspensions with a mechatronic network strut. *Veh. Syst. Dyn.* **2011**, *49*, 811–830. [[CrossRef](#)]
28. López-Martínez, J.; Martínez, J.; García-Vallejo, D.; Alcayde, A.; Montoya, F.G. A new electromechanical analogy approach based on electrostatic coupling for vertical dynamic analysis of planar vehicle models. *IEEE Access* **2021**, *9*, 119492–119502. [[CrossRef](#)]
29. Chen, M.Z.; Papageorgiou, C.; Scheibe, F.; Wang, F.-C.; Smith, M.C. The missing mechanical circuit element. *IEEE Circuits Syst. Mag.* **2009**, *9*, 10–26. [[CrossRef](#)]
30. Li, Y.A.; Cheng, Z.; Hu, N.Q.; Yang, Y.; Zhuo, X. Modeling, design and experiments of a ball-screw inerter with mechanical diodes. *J. Sound Vib.* **2021**, *504*, 116121.
31. Yang, X.; Yan, L.; Shen, Y.; Liu, Y.; Liu, C. Optimal Design and Dynamic Control of an ISD Vehicle Suspension Based on an ADD Positive Real Network. *IEEE Access* **2020**, *8*, 94294–94306. [[CrossRef](#)]
32. Shen, Y.; Hua, J.; Fan, W.; Liu, Y.; Yang, X.; Chen, L. Optimal design and dynamic performance analysis of a fractional-order electrical network-based vehicle mechatronic ISD suspension. *Mech. Syst. Signal Process.* **2023**, *184*, 2592–2601. [[CrossRef](#)]
33. Ning, D.; Du, H.; Zhang, N.; Sun, S.; Li, W. Controllable Electrically Interconnected Suspension System for Improving Vehicle Vibration Performance. *IEEE/ASME Trans. Mechatron.* **2020**, *25*, 859–871. [[CrossRef](#)]
34. Hu, Y.L.; Chen, M.Z.Q. Low-complexity passive vehicle suspension design based on element-number-restricted networks and low-order admittance networks. *J. Dyn. Syst. Meas. Control.-Trans. Asme* **2018**, *140*, 101014. [[CrossRef](#)]
35. Li, Y.; Yang, X.; Shen, Y.; Liu, Y.; Wang, W. Optimal design and dynamic control of the HMDV inertial suspension based on the ground-hook positive real network. *Adv. Eng. Softw.* **2022**, *171*, 103171. [[CrossRef](#)]
36. Shen, Y.; Hua, J.; Wu, B.; Chen, Z.; Xiong, X.; Chen, L. Optimal design of the vehicle mechatronic ISD suspension system using the structure-immittance approach. *Proc. Inst. Mech. Eng. Part D J. Automob. Eng.* **2022**, *236*, 512–521. [[CrossRef](#)]
37. Zhong, R.; Bi, C.; Chen, Y.; Chen, Z.; Zhou, A.; Yang, Z.; Zhai, J. A Simplified Method for Extracting Parasitic Inductances of MOSFET-Based Half-Bridge Circuit. *IEEE Access* **2021**, *9*, 14122–14129. [[CrossRef](#)]
38. Advani, J.; Gupta, O. Networks for a Subclass of Minimum Biquartic Impedance Functions. *IEEE Trans. Circuit Theory* **1965**, *12*, 621–622. [[CrossRef](#)]
39. Lee, S.; Frisch, I. A Class of RLC Networks with Fewer Nonreactive Elements than the Brune Realization. *IEEE Trans. Circuit Theory* **1964**, *11*, 418–421. [[CrossRef](#)]
40. Yang, X.F.; Song, H.; Shen, Y.J.; Liu, Y.L. Study on adverse effect suppression of hub motor driven vehicles with inertial suspensions. *Proc. Inst. Mech. Eng. Part D J. Automob. Eng.* **2022**, *236*, 767–779. [[CrossRef](#)]
41. Wang, F.C.; Chan, H.A. Mechatronic Suspension Design and Its Applications to Vehicle Suspension Control. *IEEE Conf. Decis. Control.* **2008**, *12*, 3769–3774.
42. Clerc, M.; Kennedy, J. The particle swarm-explosion, stability, and convergence in a multidimensional complex space. *IEEE Trans. Evol. Comput.* **2002**, *6*, 58–73. [[CrossRef](#)]